Undergraduate Honors Thesis

Analysis of Negative Stiffness Devices with Application to Vehicle Seat Suspensions

Submitted to:

The Engineering Honors Committee

As partial requirement for graduation with honors research distinction in Mechanical Engineering

199 Hitchcock Hall

College of Engineering

The Ohio State University

Columbus, Ohio 43210

Written by:

Saeid Loghavi

loghavi.3@osu.edu

Advisors: Prof. Rajendra Singh and Dr. Scott Noll

April 2015

TABLE OF CONTENTS

ABSTRACT

This research is motivated by some vehicle seat suspension designs that claim improved vibration isolation and motion control through use of snap-through devices. The geometric nonlinearity concept can be used to create negative spring stiffness and such mechanism are achieved by either a particular mechanism design or via slender beam structures. This research studies both concepts, the first one through an analytical model and the second one using a nonlinear finite element code. The nonlinear spring models are approximated via a cubic polynomial stiffness term (hardening type). Typical transient response of a single degree of freedom nonlinear system model is studied when subjected to initial conditions, ramp input, or a base excitation profile (over a limited time duration).

LIST OF FIGURES

27	29	Components of input profile from t=0.5 to t=2.5 sec
28	29	Acceleration input profile
29	30	FFT of the input signal, Fig. 28
30	32	Force-deflection curve for pre-compression study
31	33	Motion control, pre-compression study
32	34	Motion control, step (a) and ramp (b) input profile with amplitude 50 mm
33	35	Maximum displacement; Green ($^{l}/_{l_0} = 0.85$), Blue ($^{l}/_{l_0} = 0.7$)), Red ($^{l}/_{l_0} = 0.55$)
34	35	Mass acceleration; Black (linear), Green ($^{l}/_{l_0} = 0.85$), Red ($^{l}/_{l_0} = 0.55$)
35	36	Mass acceleration; Black (linear), Green ($^{l}/_{l_0} = 0.85$), Red ($^{l}/_{l_0} = 0.55$)
36	37	Force deflection, stiffness study
37	38	Motion control, stiffness study
38	38	Maximum displacement; Blue ($^{k_h}/_{k_v} = 1$)), Red ($^{k_h}/_{k_v} = 2$)
39	39	Mass acceleration, Input amplitude: 0.1 $^{\mathrm{m}}/_{\mathrm{s}^2}$
40	39	Mass acceleration, Input amplitude: 6 $^{\mathrm{m}}/_{\mathrm{s}^2}$
41	40	Force deflection, spring length study
42	41	Motion control, spring length study
43	42	Maximum displacement
44	42	Mass acceleration, Input amplitude: 2 $^{\mathrm{m}}/_{\mathrm{s}^2}$
45	43	Mass acceleration, Input amplitude: 4 $^{\mathrm{m}}/_{\mathrm{s}^2}$
46	44	Nonlinear behavior of a snap-through beam; key: Red is for steel and blue is for Aluminum
47	45	Nonlinear behavior of a snap-through beam; key: Orange is for thickness=1.1 mm and blue is for thickness=1.0 mm
48	46	Nonlinear behavior of a snap-through beam; key: Red is for width=5 mm and blue is for width=4 mm
49	47	Nonlinear behavior of snap-through beam structure; key: Orange is for steel and blue is for Aluminum
50	48	Nonlinear behavior of a snap-through beam structure; key: Orange is for thickness=1.1 mm and blue is for thickness=1.0 mm

LIST OF SYMBOLS

A	Excitation Amplitude (Oscillatory input: $\left({}^{\mathrm{m}}/_{\mathrm{s}^2}\right)$, Ramp or step input: (m))
c	Linear damping coefficient $\left(\frac{\mathrm{N.s}}{\mathrm{m}}\right)$
f_0	Fundamental (natural) frequency of a SDOF= $f_0 = \frac{1}{2\pi}\sqrt{\frac{k}{m}}$ (Hz)
$\bar{f}$	Ratio of duffing oscillator force to weight: $\bar{f} = \frac{F_D}{mg}$
F	Force (Exact force deflection equation): $F(x) = k_v x + 2k_h x\left(1 - \frac{l_0}{(x^2+l^2)^{1/2}}\right)$, (N)
F_D	Force (Duffing oscillator): $F_D = k_1 x + k_3 x^3$, (N)
F_h	Force (Horizontal Spring): $F_h(x) = k_h\left(\sqrt{l^2 + x^2} - l_0\right)$, (N)
k_1	First Stiffness Coefficient as in Duffing's oscillator: $F_D = k_1 x + k_3 x^3, \left(\frac{\mathrm{N}}{\mathrm{m}}\right)$
k_3	Second Stiffness Coefficient as in Duffing's oscillator: $F_D = k_1 x + k_3 x^3, \left(\frac{\mathrm{N}}{\mathrm{m}^3}\right)$
k_h	Stiffness of horizontal spring $\left(\frac{\mathrm{N}}{\mathrm{m}}\right)$
k_v	Stiffness of vertical spring $\left(\frac{\mathrm{N}}{\mathrm{m}}\right)$
l	Length of horizontal spring at static equilibrium (m)
l_0	Free length of horizontal spring (m)
m	Effective mass of the seat and operator (kg)
U_1	Displacement in the x direction (FEM)
U_2	Displacement in the y direction (FEM)
U_3	Displacement in the z direction (FEM)
U_{R1}	Rotation about the x axis (FEM)
U_{R2}	Rotation about the y axis (FEM)
U_{R3}	Rotation about the z axis (FEM)

$u(t)$	Input (ramp, step or oscillatory)
x	Position of the mass (m)
$\bar{x}_a$	Dimensionless deflection of the mass when normalized by the static deflection due to weight= $\bar{x}_a = \frac{x}{x_s}$
x_s	Deflection of the system due to the weight (m)
y	Position of the base (m)
z	Relative position of the mass and base= $z = x - y$ (m)
z_a	Dimensionless relative displacement when normalized by the maximum deflection of the base from its equilibrium position= $\bar{z}_a = \frac{z}{y_{max}}$
z_{max}	Maximum dimensionless relative displacement when normalized by the maximum deflection of the base from its equilibrium position= $\bar{z}_{max} = \max(\bar{z}_a)$

LIST OF ABBREVIATIONS

SDOF	-	Single degree of freedom system
HSLDS	-	High Static Low Dynamic Stiffness
FEM	-	Finite Element Model

1. INTRODUCTION

1.1. Motivation

Operators of many in road and off road vehicles are exposed to whole body vibrations. The low frequency (0.5-5 Hz) range is most harmful to human health and activity as the human body exhibits high sensitivity to vibration in these frequencies [1]. Vibration isolation devices are used to reduce the fundamental frequency f_0 below 0.5 Hz. As shown in Figure 1, a review of a single degree of freedom system (SDOF) reveals that the fundamental frequency of the system is,

$$f_0 = \frac{1}{2\pi}\sqrt{\frac{k}{m}} \text{ (Hz)} \tag{1}$$

where k is the system equivalent stiffness and m is the mass of the base supported by the load bearing element and occupant. Reducing the fundamental frequency can be achieved by lowering the stiffness of the system.

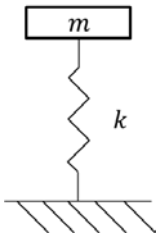

Figure 1: Single degree of freedom linear, undamped system with mass *m* and stiffness *k*

Seat suspensions are designed to attenuate vibrations experienced by operators of commercial vehicles such as class eight trucks. Seat suspensions are complex structures with significant non-linear characteristics and are therefore difficult to model. As shown in Figure 2, seat suspensions are comprised of springs, dampers and in some applications hydraulic and pneumatic components.

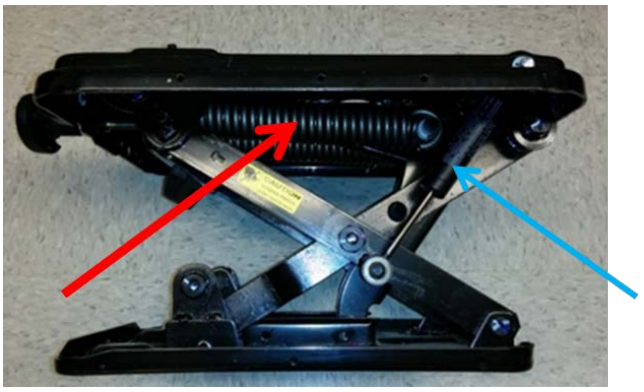

Figure 2: KAB seat suspension, red: Linear spring, blue: Damper [Picture taken by OSU]

A new or a modified existing seat design must undergo standardized laboratory tests prior to use in commercial vehicles. The testing is time consuming and costly and may not provide detailed information regarding possible improvements in the design [2]. Development of a reduced order mathematical model for seat suspensions should provide good insight and intuition about the dynamic response. Prior work [2] on reduced mathematical models for seat suspension applications has focused on using two different models. First, lumped parameter model assembly employs the dynamic properties of each component such as mass and stiffness and therefore requires separate measurement of each of the components. Simplified lumped parameter models are often best suited for the development of a particular seat suspension. Second, in the Bouc-Wen model [2] the dynamic characteristics of the seat suspension and seat are described by a single Bouc-Wen equation. The coefficients of the Bouc-Wen equation are obtained by minimizing the difference between predicted and measured accelerations of a load supported in the seat [2]. The Bouc-Wen model may provide a useful simulation of an existing seat and assist in optimization of an individual component in the seat [2].

One of the major components of seat suspensions is linear springs. Springs are the major load bearing element in the system and therefore lowering the stiffness (k) of the spring will result in large static deflections during initial loading of the seat suspension. This limitation of linear

stiffness elements requires the use of nonlinear devices in vibration isolation devices. One such nonlinear system is the negative stiffness spring.

Negative stiffness concept may be used to cancel or minimize the stiffness of a vehicle suspension. Drastic reduction in stiffness would magnify the role of damping inherent in the system; this would suggest a means for achieving high hysteretic damping [3]. High structural damping is more desirable than high viscous damping because it can limit resonant peaks without significantly reducing isolation efficiency beyond resonance [3]. A spring with negative stiffness has no load capacity; however it can operate while connected in parallel with mechanical, hydraulic, pneumatic, or other load-bearing springs with positive stiffness [1] as shown in Figure 3.

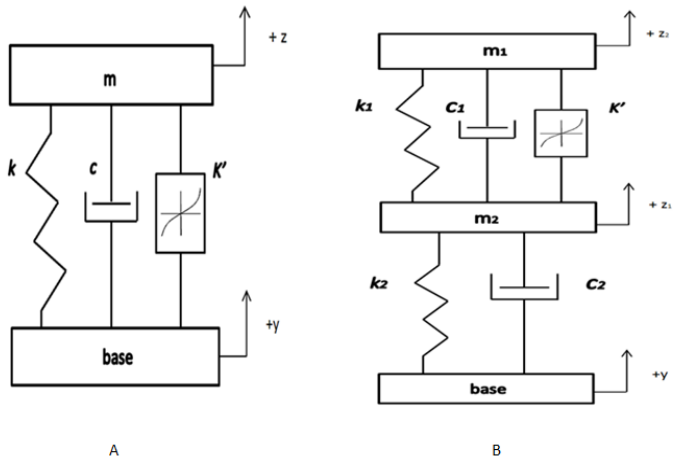

Figure 3: Nonlinear mechanical system models with base excitation y(t). (A) SDOF system (B) Two Degree of freedom system

1.2. Research objectives:

This research attempts to analyze few negative stiffness concepts that are discussed in the literature or patents exploit geometric nonlinearities to improve isolation and motion control. The specific objectives include the following: (i) Analyze a snap-through mechanism leading to a

nonlinear spring components, (ii) Develop a finite element modeling procedure to analyze snap-through beam structures, (iii) Develop a simplified mathematical model of the nonlinear snap-through mechanism and incorporate the model into a single degree of freedom (SDOF) system and; (iv) Analyze the dynamic performance of the snap-through mechanism and compare the results to the dynamic performance of an equivalent linear system. The snap-through beam structures are designed and analyzed using finite element software ABAQUS/CAE [4].

2. REVIEW OF SOME PATENTS

The use of negative stiffness springs for vibration isolation goes back to at least the 1960s. Lee et al. [1] provided designers with comprehensive design guidelines that allows the alteration of the performance and size of the negative stiffness spring by changing the design parameters. Carrella et al. [5] analyzed the system performance under steady state conditions.

Traditionally rod shaped elastic structures were and remain a benchmark for negative stiffness springs [1]. Multiple patents by Goverdovskiy et al. [6,7,8], outline the steps required to elastically deform a beam in order to reach a bistable configuration with nonlinear characteristics.

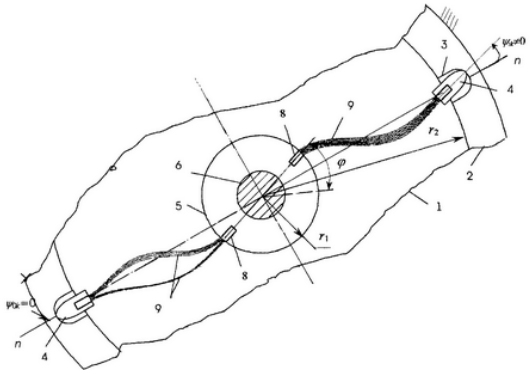

Figure 4: Negative stiffness device as displayed in a patent by Goverdovskiy et al. [8]

In the first step, a simply supported slender beam is subjected to axial load F1 resulting in buckling of the beam and reduction in the length as shown in Figure 5A. A small lateral force (0.05 F1) is also applied to the mid-point of the beam to allow the beam to buckle in the desired direction. In the second step, the forces from the first step are replaced with a bending moment (T1). Changing the boundary conditions and restricting the motion of the beam in the axial direction results in the shape shown in Figure 5B. In the third step, boundary conditions are changed and both sides of the beam are clamped as shown in Figure 5C. In the fourth step, bending moment is replaced with a lateral force (F2) applied at the mid-point of the beam which results in the beam snapping through as shown in Figure 5D. In order to achieve the desired result to produce a non-linear spring, key parameters of the model (including beam geometry, force and bending moment magnitudes) must be modified until buckling in step one and snap-through in the final step are achieved. Thus, the structure is geometrically non-linear.

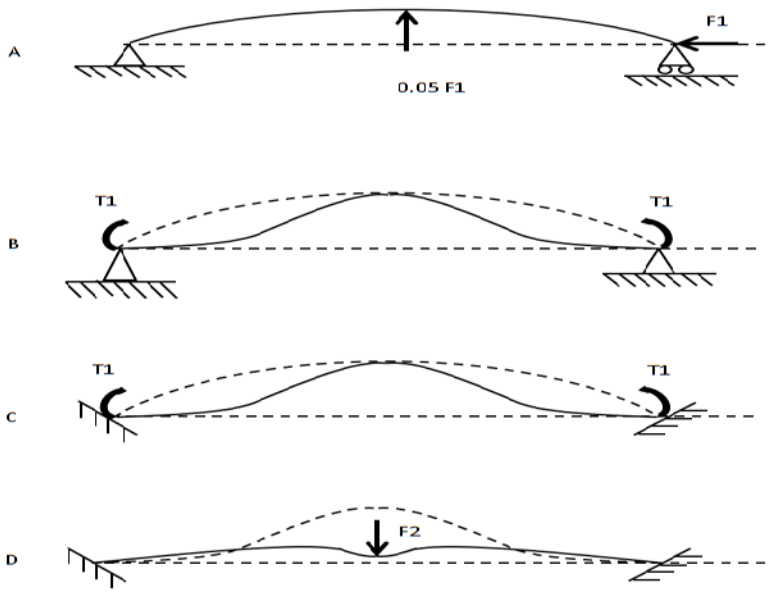

Figure 5: Steps needed to achieve a negative stiffness spring element using a slender beam [1]. (A) Apply axial and lateral forces (F1 and 0.05F1) to induce buckling. (B) Apply bending moment (T1) and remove forces. (C) Remove all degrees of freedom. (D) Apply lateral force (F2) and remove bending moment.

Slender beams of Figure 5 can be implement into a mechanism with multiple components [1] as shown in Figure 6. The design of the mechanism translates the lateral motion of the seat suspension to a torsional load. The nonlinear behavior of the negative stiffness component lowers the linearized stiffness of the system about an operating point.

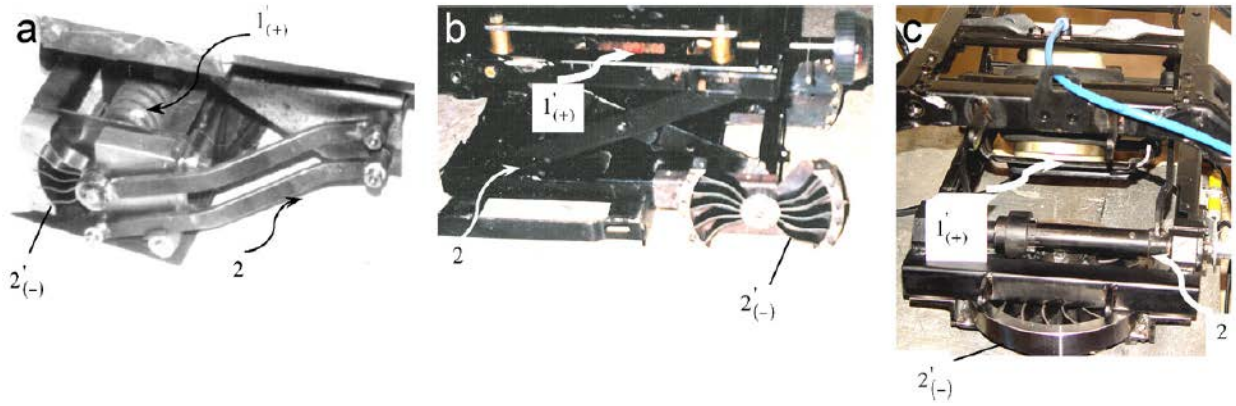

Figure 6: Upgraded seat suspensions from [1]: (a,b) layouts of mechanical and (c) pneumatic suspensions, here $\mathbf{1}'_{(+)}$ are load bearing elements; $\mathbf{2}'_{(-)}$ are the mechanisms with negative stiffness, and 2 are guide mechanisms.

3. SNAP THROUGH MECHANISM ANALYSIS USING A SIMPLE MODEL

In order to develop a mathematical representation of a SDOF model with reduced stiffness a snap-through device is proposed in Figure 7. This model is produced by combining two sub-systems, one shown in Figure 8.a with positive stiffness and one with negative stiffness shown in Figure 8.b.

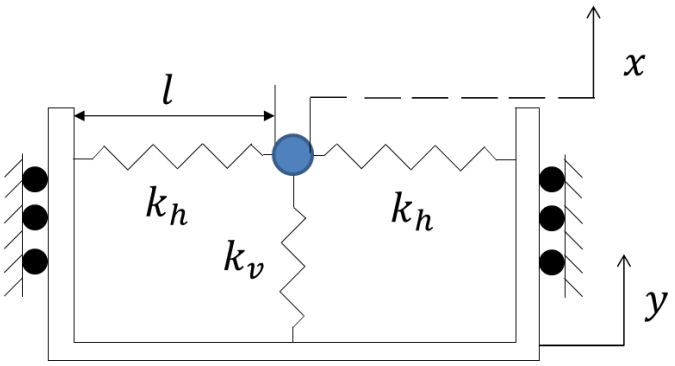

Figure 7: SDOF base excitation model of a snap-through device with reduced stiffness

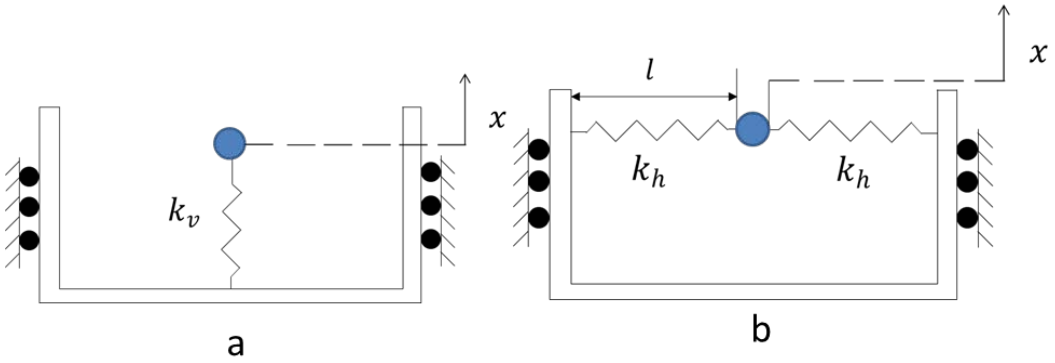

Figure 8: SDOF model with a) positive stiffness, b) negative stiffness

A free body diagram of the side spring (k_h) is shown in Figure 9. Due to vertical displacement, x, the effective length of the spring will increase to $\sqrt{l^2 + x^2}$ where l is the length of spring at the static equilibrium.

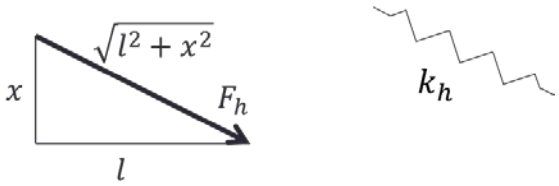

Figure 9: Free body diagram of side spring

Assuming the free length of the spring is l_0, the horizontal spring force (F_h) is found as

$$F_h(x) = k_h\left(\sqrt{l^2 + x^2} - l_0\right). \tag{2}$$

Using the geometry of the system, the vertical component of the spring force F_{hx} is

$$F_{hx}(x) = F_h\left(\frac{x}{\sqrt{l^2 + x^2}}\right) = k_h x\left(1 - \frac{l_0}{\sqrt{l^2 + x^2}}\right) \tag{3}$$

is obtained. Considering that the system shown in Figure 7 contains two side springs k_h and one vertical spring k_v, the overall spring force for the reduced stiffness model is derived as

$$F(x) = k_v x + 2k_h x\left(1 - \frac{l_0}{(x^2 + l^2)^{1/2}}\right). \tag{4}$$

In derivation of equations 2-4, it is assumed that the lateral spring rate is negligible and only axial forces are considered.

To display the effects of the negative stiffness component on the overall stiffness of the mechanism, force deflection plots of the system are generated in Figure 10 where $\bar{f} = \frac{F}{mg}$, $\bar{x}_a = \frac{x}{x_s}$ and $x_s = \frac{mg}{k_v}$. $m = 58$ kg is the mass being supported and $g = 9.81\ \frac{\text{m}}{\text{s}^2}$ is the acceleration due to gravity.

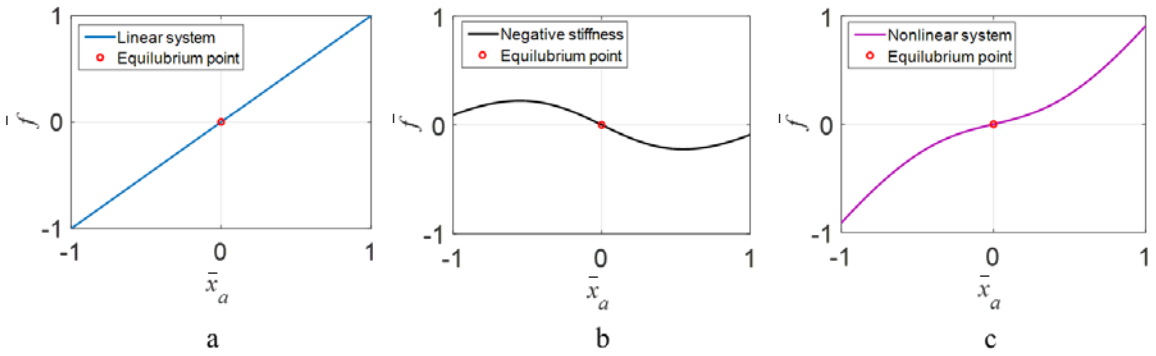

Figure 10: Force deflection (a) for linear model (Fig 8a), (b) for nonlinear model (Fig 8b), (c) for the reduced stiffness model of (Fig 7)

In development of the SDOF model, at the static equilibrium, the side springs can be pre-compressed, left at neutral position or put in tension as shown in Figure 11. If length of the spring at equilibrium l is chosen to be larger than the free length ($l > l_0$) the system is always under tension and therefore the equivalent stiffness is larger than from a linear model. If the free length and the equilibrium length are chosen to be equal ($l = l_0$), the system is stable at the equilibrium point however motion will result in increased tension and therefore the system will have larger stiffness than from a linear model. If the system is designed with pre-compression ($l < l_0$), the side spring has two stable points, one on each side of the equilibrium point. This bistable configuration allows for the nonlinear behavior of the side springs as shown in Figure 10 b.

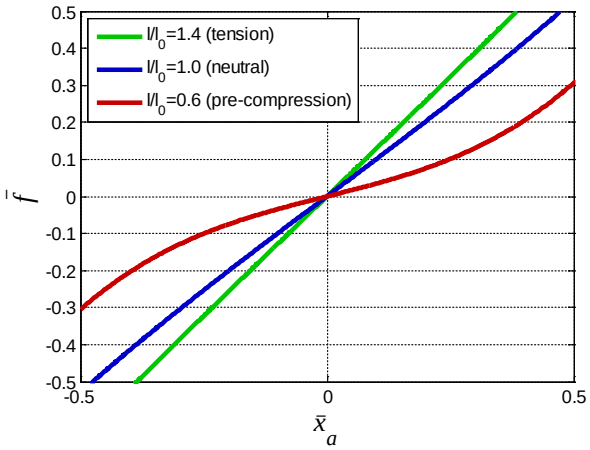

Figure 11: Force deflection curve, nonlinear system

4. ANALYSIS OF SNAP THROUGH BEAM STRUCTURE

Nonlinear spring elements are constructed and analyzed using finite element models developed from slender beams using the following steps: (i) Short shell element is created and simply supported on both sides (Fig 12 a), (ii) An axial displacement is applied to the right side and a lateral displacement is applied to the center (Fig 12 b), (iii) Equal moment is applied to both sides

of the beam (Fig 12 c), (iv) Both sides of the beam are fixed and torque is removed, (v) A lateral displacement is applied to the center, causing the beam to snap-through (Fig 12 d). These steps essentially duplicate the design procedures outlined in patents by Goverdovskiy [6,7,8].

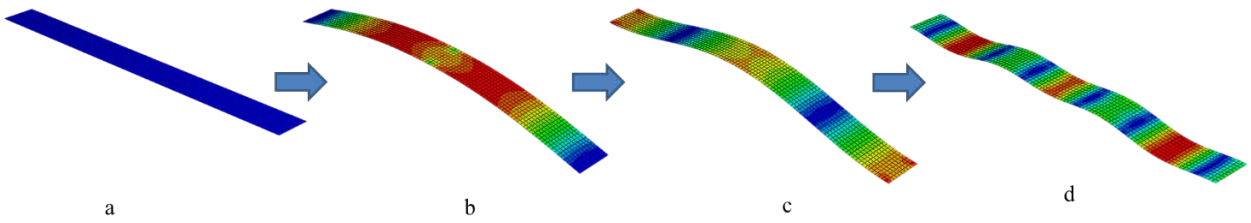

Figure 12: FEM steps needed to create a snap-through element using a slender beam

The nonlinear behavior of the beam resulting in negative stiffness is due to the snap-through in step (v). The nonlinear behavior of the system is however a function of the beam geometry, material properties, moment and displacement applied in steps (ii) and (i) respectively.

An example for the FEM of the beam element is as follows: The beam is made from Aluminum with elastic modulus, $E = 69 \times 10^9 \text{Pa}$, Poisson's ratio, $v = 0.33$ and density $\rho = 2700 \ \frac{\text{kg}}{\text{m}^3}$. The beam is created as a shell element with length 50 mm, thickness 1 mm, and width 5 mm. A partition line is created at the center which is used for application of lateral displacement.

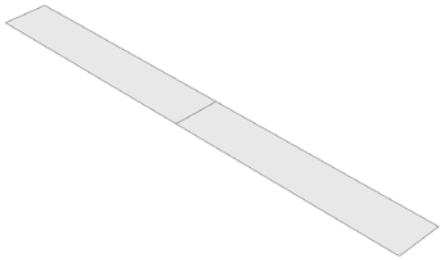

Figure 13: Beam geometry and partition in the FEM

In the first step the following boundary conditions are applied: The left side ($U_1 = U_2 = U_3 = 0$), the right side ($U_1 = -1$ mm , $U_2 = U_3 = 0$), and the center partition ($U_1 = -0.5$ mm , $U_2 = 4.3$ mm , $U_3 = 0$). Here U_1, U_2 and U_3 are the displacements in x, y and z directions respectively. In this step the rotational degrees of freedom are unconstrained.

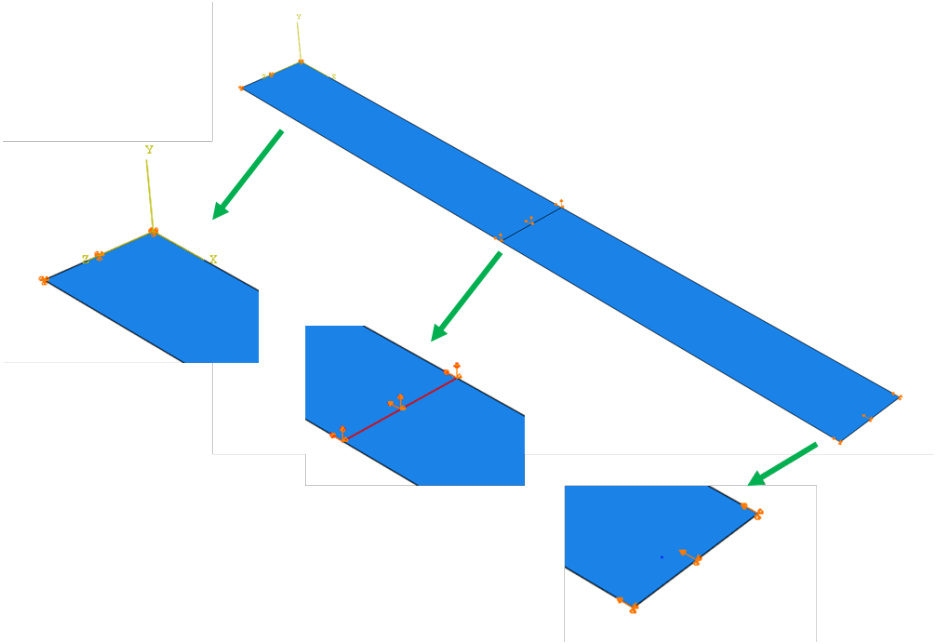

Figure 14: Initial boundary conditions in FEM

Before applying a moment on the two sides of the beam, a step is created to free the displacement boundary conditions from the center partition in the U_1 and U_2 directions. In the next step an equal moment of 200 N. m is applied to both left and right sides by using shell edge load as the load type.

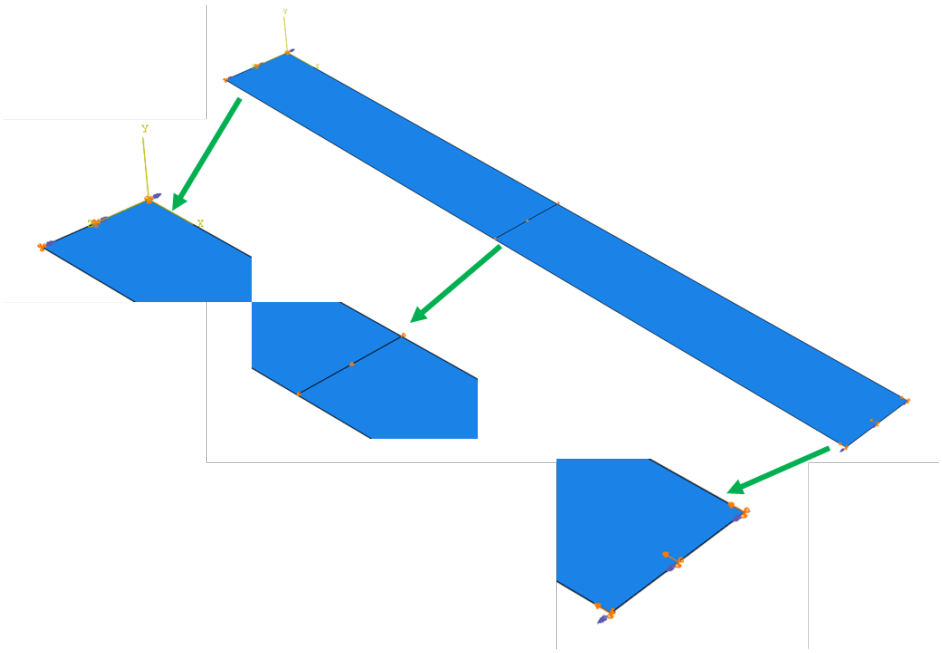

Figure 15: Moment application in FEM

The next step is to fix both sides of the beam: the left side ($U_1 = U_2 = U_3 = U_{R1} = U_{R2} = U_{R3} = 0$), and the right side ($U_1 = -1\ mm\ , U_2 = U_3 = U_{R1} = U_{R2} = U_{R3} = 0$), where U_{R1}, U_{R2} and U_{R3} are rotations about x, y and z axis respectively.

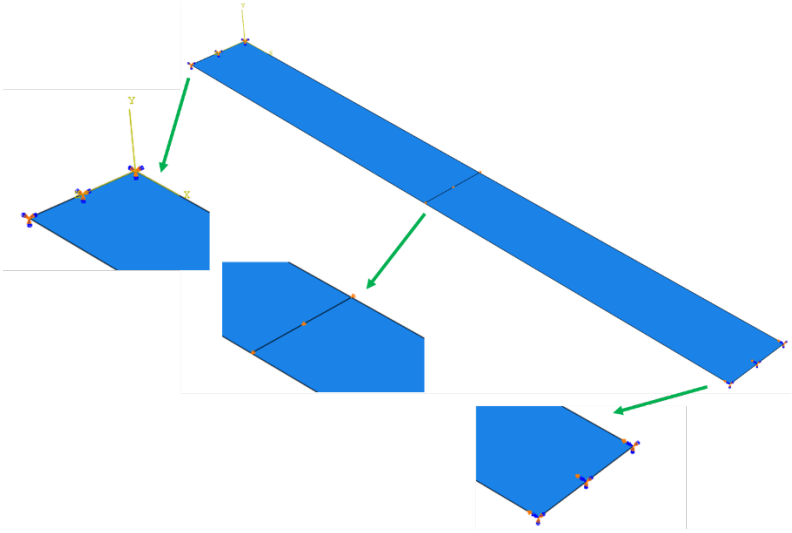

Figure 16: Fixed sides in FEM

In the final step, a lateral displacement is applied to the center partition pushing the center in y direction down from $4\ \text{mm}$ to $0.5\ \text{mm}$ which creates a snap-through condition. The nonlinear behavior of the beam is shown in Figure 17. In the final step of finite element analysis, the beam is preloaded to a positive displacement of 4mm. From that point, the beam is deflected downward. The stiffness of the beam is initially positive and as the beam is pushed down, the stiffness is reduced until stiffness becomes zero and later starts to become increasingly negative.

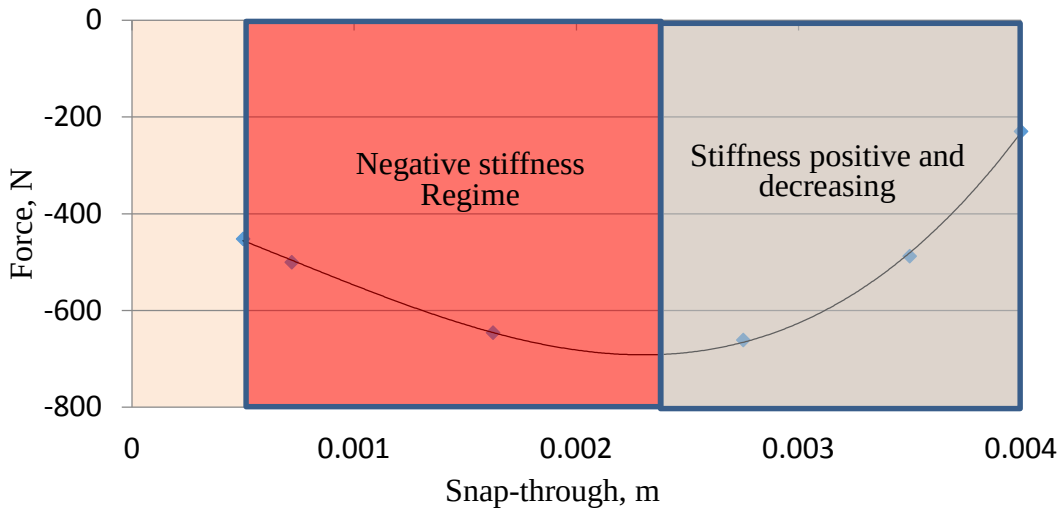

Figure 17: Nonlinear behavior of a snap-through slender beam in the final step of FEM, beam initially preloaded to 4 mm and pushed down to 0.5 mm

It is assumed that during static deflection, negative stiffness devices designed using beam elements, are deflected to the point where beam has zero stiffness. This will allow the device to enter negative stiffness region once an input is applied into the system. Based on this assumption, the equilibrium point for negative stiffness devices designed using beam elements is defined as the point where device is deflected to zero stiffness.

Due to the limited space available in seat suspensions for negative stiffness devices, using a single beam is not efficient. To improve the packaging and efficiency of the device, patents [6,7,8] show the use of multiple beams as shown in Figure 6. For instance, the lateral motion of the seat suspension is translated to a rotation which is applied at the central ring. To study the performance of these devices in the next step of the finite element analysis, six beams following the steps outlined are packaged into a single device as shown in Figure 18. The diameter of the central ring is 20 mm.

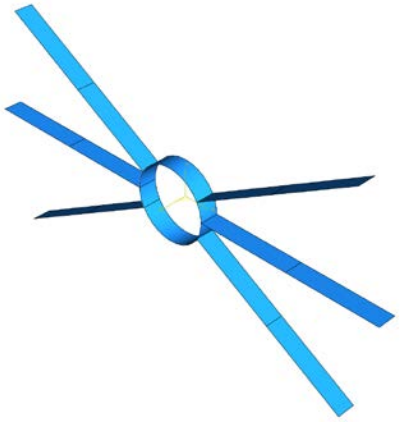

Figure 18: Negative stiffness device with six beam elements around a ring using FEM

The difference in using the device and the beam to achieve negative stiffness is in the final step in which a rotation is applied to the central ring. Figure 19 shows the deformation of the device as rotation is applied.

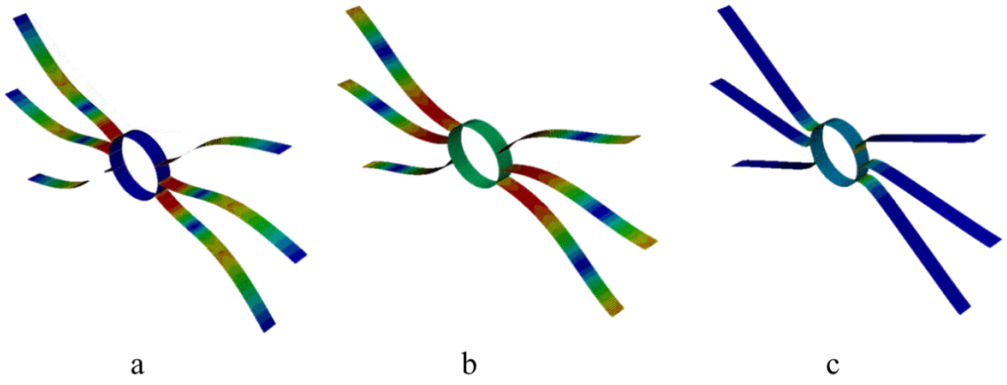

Figure 19: Rotation applied to the center ring with (a) 0 degrees, (b) 40 degrees, (c) 80 degrees

The nonlinear behavior of the device is shown in Figure 20. The behavior of the device is similar to that of the single beam with a positive initial negative which is reduced due to increased rotation until the effective stiffness of the device becomes zero and later starts to become increasingly negative.

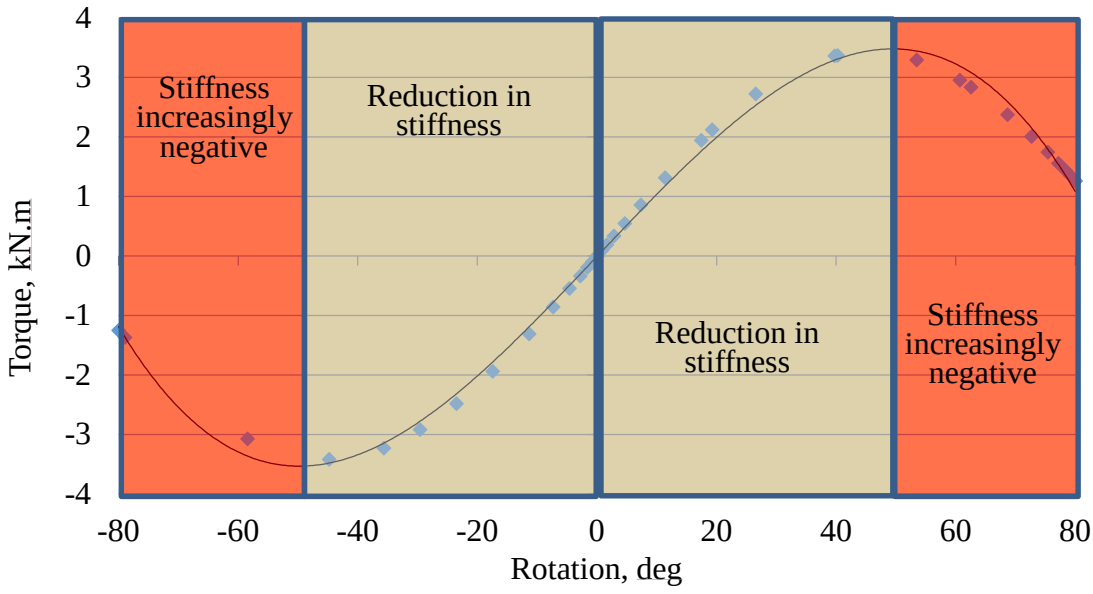

Figure 20: Nonlinear behavior of snap-through beam structure of Figures 18 and 19

It is assumed that during static deflection, negative stiffness devices designed using multiple beam elements and the central ring, are deflected to the point where the device has zero stiffness. This will allow the device to enter negative stiffness region once a torque input is applied into the system. Based on this assumption, the equilibrium point for negative stiffness devices designed using multiple beam elements is defined as the point where the device has zero stiffness.

The SDOF model with base excitation shown in Figure 7 is developed in order to study dynamic performance of isolation devices which use snap-through beam structure shown in Figure 18. As shown in Figure 21, as the SDOF model goes through displacement x, a compliant mechanism with arm length L, can be attached to the point mass. The compliant mechanism converts the lateral displacement of the SDOF model to a rotation which may apply a torque T. Under small displacements, it may be assumed that multiplying the force deflection equation for the vertical component of force for the side springs (described by equation 3) by length of the arm L,

$$T = L \times F_{hx}(L\theta) = L \times F_h\left(\frac{L\theta}{\sqrt{l^2 + (L\theta)^2}}\right) = L \times k_h \times L\theta\left(1 - \frac{l_0}{\sqrt{l^2 + (L\theta)^2}}\right). \quad (5)$$

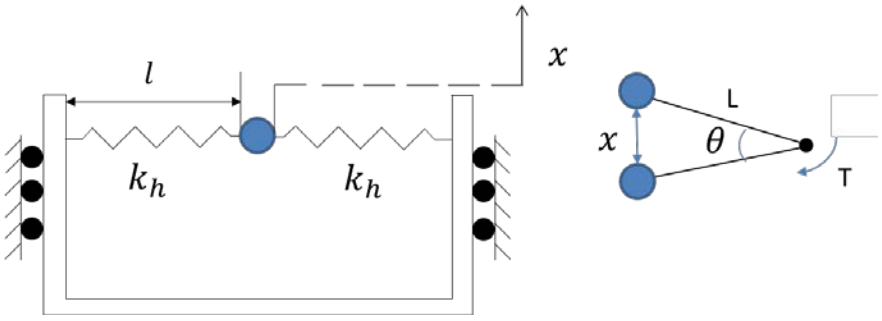

Figure 21: Analogous behavior: SDOF model and snap through beam structure (Figure 18)

Plotting torque vs. angle of rotation for equation 5, Figure 22, shows that using the compliant mechanism the nonlinear behavior of the snap-through structure, in the negative stiffness region, is similar to that of the side springs in the SDOF model.

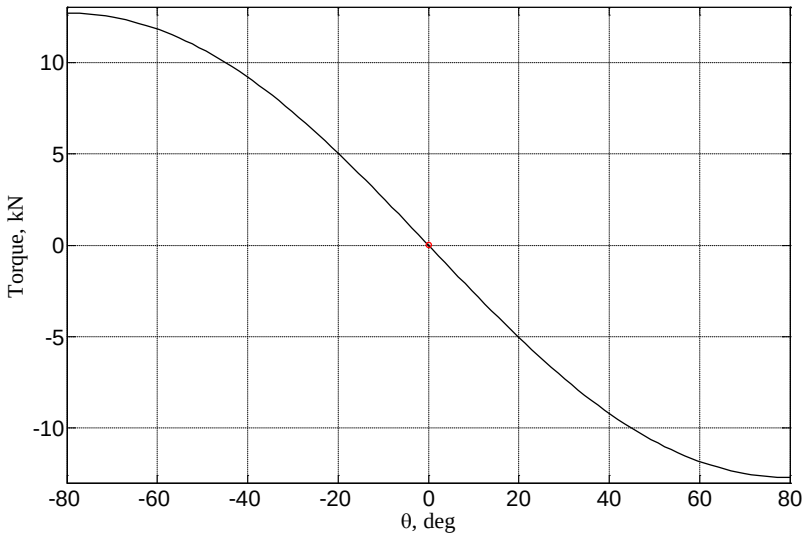

Figure 22: Torque vs. Angle of rotation, SDOF model with compliant mechanism

5. SIMPLIFIED SDOF MODEL

An analytical model of a seat suspension mechanism is generated as shown in Figure 23. Key system parameters include the following: (i) the stiffness of the equivalent linear system k_v, the equivalent mass of the operator and seat cushion m and the damping coefficient of the seat suspension c are obtained from measured stiffness of a seat suspension designed for an industrial truck; these values are provided in [2]. (ii) The coordinates x and y are used to represent the position of the mass and the base respectively. (iii) The stiffness of side springs k_h and the length of the spring at equilibrium l are chosen considering the physical constraints of the system such as the space available and results obtained from transient simulations.

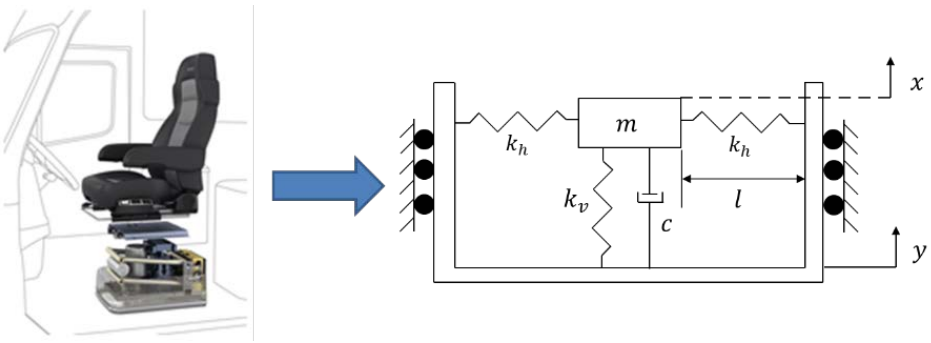

Figure 23: Mechanism with negative stiffness

Since Equation 4 for the reduced stiffness model is complex, a simpler equation is employed for the characterization of negative stiffness. The following elastic deflection equation is for a Duffing's oscillator [5],

$$F_D(x) = k_1 x + k_3 x^3 \tag{6}$$

where the first coefficient k_1 associated with the linear term, is estimated by,

$$k_1 = k_v - 2k_h\left[\left(\frac{l_0}{l}\right) - 1\right],\ {}^{\mathrm{N}}/_{\mathrm{m}} \tag{7}$$

and the second coefficient k_3 associated with the nonlinear (cubic) term, is estimated by,

$$k_3 = k_h\left(\frac{l_0}{l^3}\right),\ {}^{\mathrm{N}}/_{\mathrm{m}^3}. \tag{8}$$

This estimate is valid for small deformations as the error in the estimate increases with an increase in deformation. Figure 24 compares the exact force-deflection (equation 4) and the approximate force-deflection (equation 6) where $\bar{f} = \frac{F}{mg} \cong \frac{F_D}{mg}$.

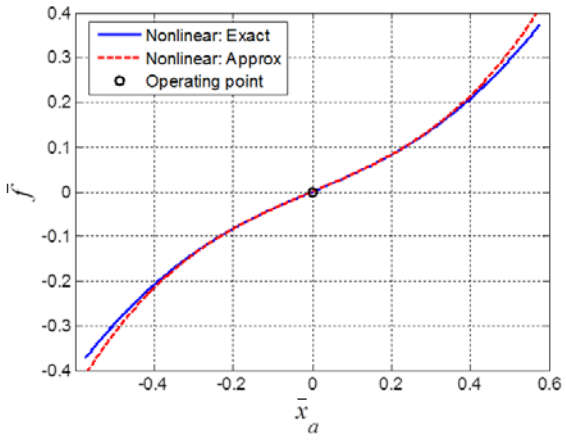

Figure 24: Comparison between the exact force-deflection (equation 4) and Duffing's oscillator (equation 6)

The next step in developing a mathematical model of the snap through mechanism is to use the free body diagram of the mass shown in Figure 25 to derive the equations of motion. An assumption for the SDOF system is that the model is at static equilibrium when the side springs are horizontal. Vertical spring k_v is compressed due to the weight prior to reaching static equilibrium.

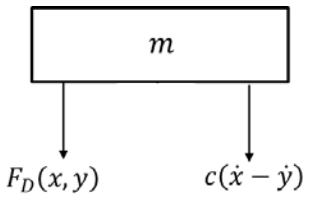

Figure 25: Free body diagram, mass

Defining $z = x - y$, as the relative displacement between the mass and the base, equation describing the motion,

$$m\ddot{z} + c\dot{z} + F_D(z) = -m\ddot{y} \tag{9}$$

is obtained. In order to keep track of the position of mass and the base, equation 9 is written in terms of variables x and y,

$$m\ddot{x} + c(\dot{x} - \dot{y}) + k_1(x - y) + k_3(x - y)^3 = 0 \tag{10}$$

solving for $\ddot{x}$,

$$\ddot{x} = -g - \frac{c(\dot{x} - \dot{y}) + k_1(x - y) + k_3(x - y)^3}{m} \tag{11}$$

is obtained. It is also assumed that the effect of viscous damping from seat dissipation mechanism is much greater than structural damping.

To obtain the position, velocity and acceleration of the mass and the base, equation of motion is written in state variable from,

$$\dot{\mathbf{X}} = \mathbf{s}(x, y, t) + \mathbf{U}(t) \tag{12}$$

where $\dot{\mathbf{X}}$ is defined as,

$$\dot{\mathbf{X}} = \begin{bmatrix} \frac{dx}{dt} \\ \frac{dy}{dt} \\ \frac{dv_x}{dt} \\ \frac{dv_y}{dt} \end{bmatrix} \tag{13}$$

and $U(t)$ is the input into the system. The three input profiles used to study the dynamic performance of the SDOF model,

$$\mathbf{U}(t) = \begin{cases} \ddot{y}(t) = A\,sin\,\omega t\,cos\,8\omega t \\ y(t) = \begin{cases} A & 2.5 > t > 0.5 \\ 0 & t < 0.5, t > 2.5 \end{cases} \\ y(t) = \begin{cases} A(t-0.5) & 2.5 > t > 0.5 \\ 2A & t > 2.5 \\ 0 & t < 0.5 \end{cases} \end{cases} \tag{14}$$

are in the form of base excitation.

In previous work by Gunston et al. [2], the input profile used to study the dynamic performance of a seat suspension was based on vehicle cab floor motion measurements when the off-road vehicle passes over an obstacle. A reproduction of acceleration measurements is shown in Figure 26.

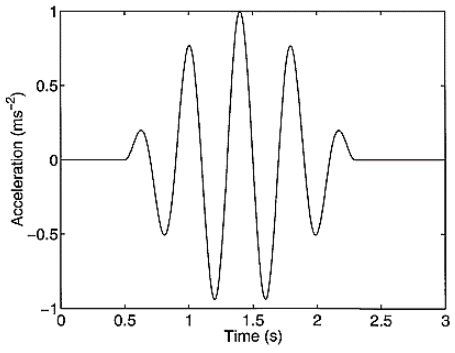

Figure 26: The base acceleration input used to measure the dynamic performance of seat suspensions [2]

Acceleration input profile shown in Figure 26 can be represented by two sinusoidal functions. One function goes through 4.5 cycles in about 2 (with a frequency of 2.25 Hz) seconds while the magnitude of the signal goes through a half cycle in 2 seconds (with a frequency of 0.5 Hz).

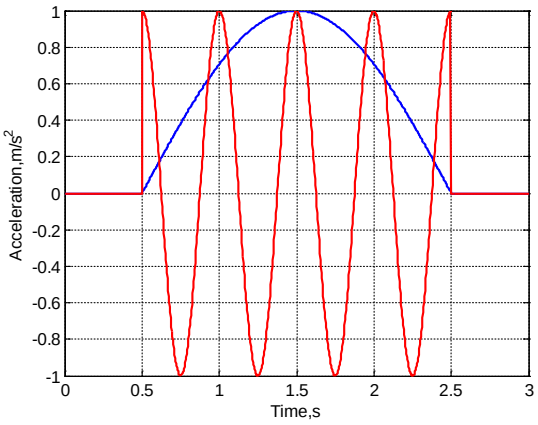

Figure 27: Components of input profile from t=0.5 to t=2.5 sec; Blue: Time-varying Amplitude (half cycle), Red: Oscillations (4.5 cycles)

The acceleration input profile is created by multiplication of the two sinusoidal functions,

$$\ddot{y}(t) = A\,sin\,\omega t\,cos\,8\omega t \qquad 0.5 < t < 2.5 \text{ sec} \tag{15}$$

where A is the amplitude of the acceleration input and ω is the circular frequency (rad/s). Choosing $\omega = \frac{\pi}{2}\ {}^{\text{rad}}/_{\text{s}}$ the acceleration input profile is shown in Figure 28. Based on an FFT analysis of the input signal, the frequency content is between 1.5 and 2.5 Hz.

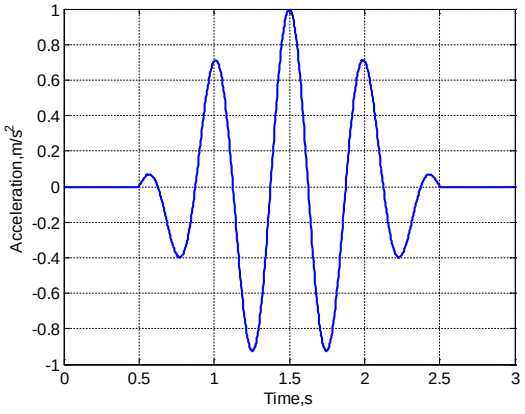

Figure 28: Acceleration input profile

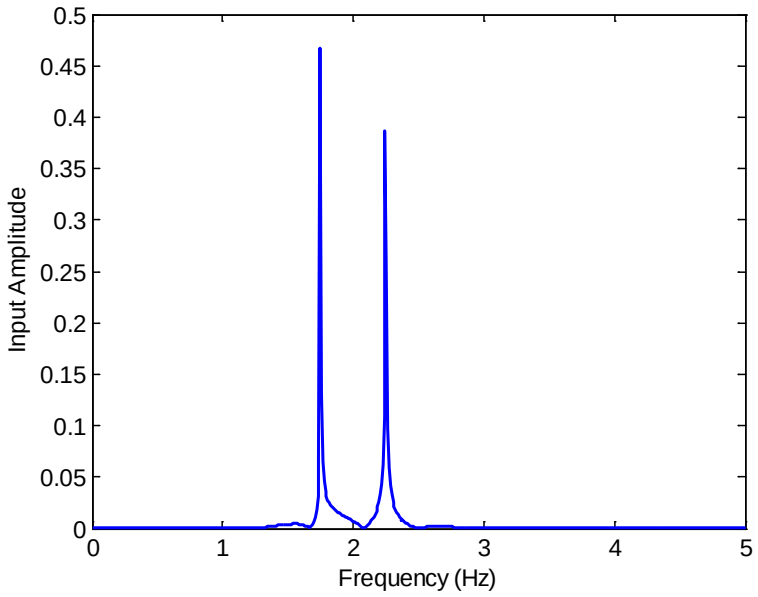

Figure 29: FFT of the input signal, Fig. 28

To study the dynamic performance of the simplified mathematical model, three types of input are used including the input profile shown in Figure 28. The equations of motion in the state variable format for the input profile with equation 15 is,

$$\begin{bmatrix} \frac{dx}{dt} \\ \frac{dy}{dt} \\ \frac{dv_x}{dt} \\ \frac{dv_y}{dt} \end{bmatrix} = \begin{bmatrix} v_x \\ v_y \\ -g - \frac{c(v_x - v_y) + k_1(x-y) + k_3(x-y)^3}{m} \\ 0 \end{bmatrix} + \begin{bmatrix} 0 \\ 0 \\ 0 \\ A\,sin\,\omega t\,cos\,8\omega t \end{bmatrix} \tag{16}$$

where,

$$v_y = A\left(\frac{9\,cos(7\omega t) - 7\,cos(9\omega t)}{126\omega}\right) \tag{17}$$

is derived by integration of the equation 15. Two other input profiles are step and ramp displacement inputs which are applied from the base.

6. SDOF SYSTEM MODEL RESULTS AND DISCUSSION

6.1. Pre-compression study

To achieve negative stiffness using the simple mathematical model shown in Figure 23, the side springs (k_h) are pre-compressed though a change in the amount of pre-compression in the spring will alter the device performance as shown in Figure 30. All three cases shown in Figure 30 have their lowest stiffness at the equilibrium point and stiffness increases as more deflection is applied. Increasing the pre-compression in the side springs results in the greater reduction in the stiffness at the equilibrium point. The increase in stiffness away from the equilibrium point is also faster for the case with the largest pre-compression. This combination is favorable in providing motion control because lowering the stiffness at the equilibrium point results in improved isolation and the increase in stiffness away from the equilibrium point prevents the system to go through large deformations. On the other hand, taking the derivative of equation 6 for the force deflection, the equation describing the equivalent stiffness of system,

$$K(x) = k_1 + 3k_3x^2, {}^{N}/_{m} \tag{18}$$

shows that the addition of the side springs results in a reduction in stiffness at equilibrium point (equation 7 shows that due to the pre-compression in the springs, k_1 is smaller than k_v) however the introduction of k_3 term away from the equilibrium point results in an increase in stiffness. In cases with larger input amplitude the increase in stiffness causes a shift in fundamental frequency of the system toward higher frequencies which can reduce the frequency range for vibration isolation.

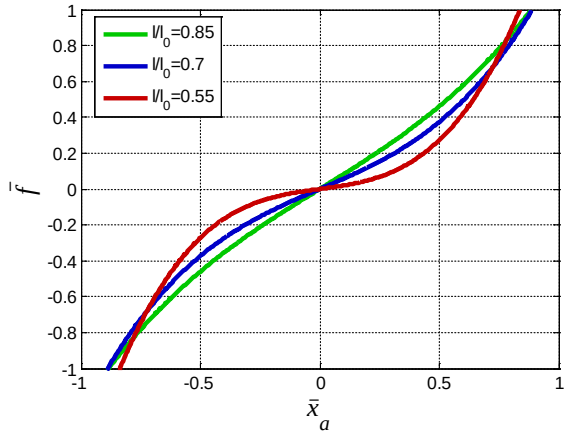

Figure 30: Force-deflection curve for pre-compression study

In order to verify the observation from the force deflection curve, the system response to the acceleration input shown in Figure 28 with amplitude of $A = 1\ {}^{\mathrm{m}}/_{\mathrm{s}^2}$, is studied. Figure 31 compares the displacement output of three different nonlinear models against the equivalent linear system with stiffness k_v, where $\bar{z}_a = \frac{z}{y_{max}}$ and y_{max} is the maximum base displacement. As shown in Figure 30, the system with greatest pre-compression has the smallest equivalent stiffness at the equilibrium point and the sharpest increase in stiffness away from equilibrium. Under small amplitude input, the nonlinear system with largest pre-compression can provide improved isolation due to the reduced stiffness while it prevents large displacement due to increased stiffness away from the operating point.

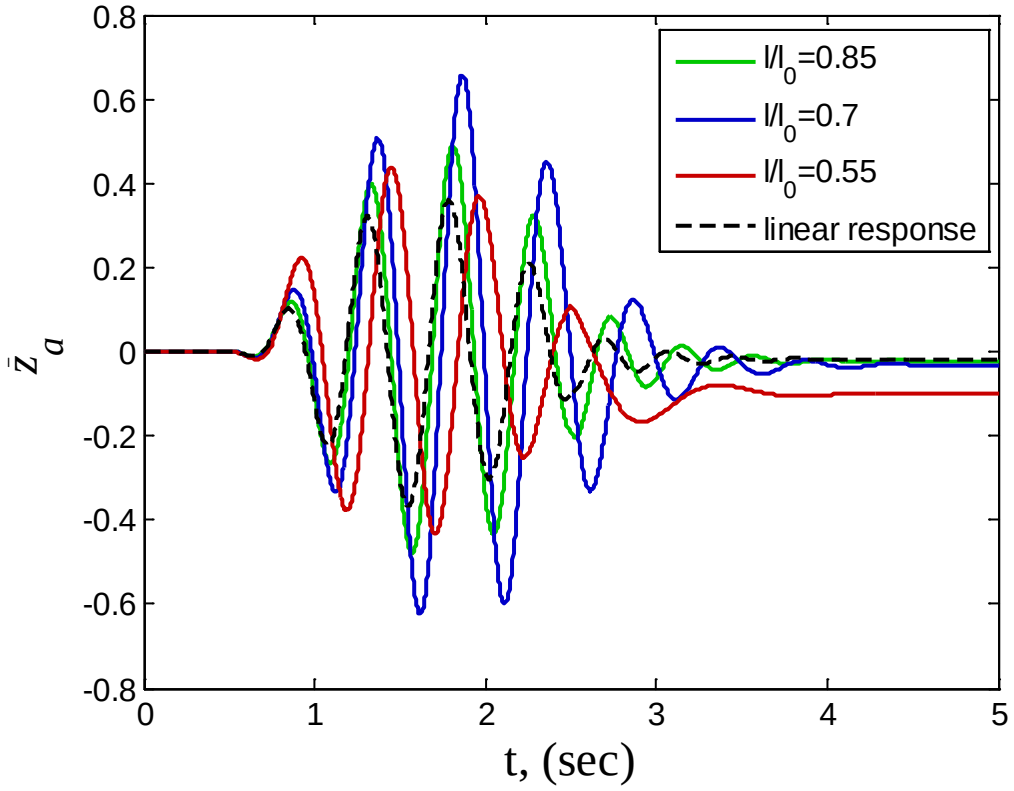

Figure 31: Motion control, pre-compression study

Large relative displacement can result in discomfort for the user. As shown in Figure 31, the linear system, due to its larger stiffness can limit the amount of displacement, however the introduction of the side springs results in reduced stiffness which may lead to large displacement. Comparing the three different nonlinear cases in Figure 31, shows that increased pre-compression can improve motion control as stiffness away from the equilibrium point is increased. Motion control can also be characterized by observing the displacement output of the system to step and ramp input profiles. Figure 32, shows the response of the SDOF model to a step (Fig. 32 a) and ramp (Fig. 32 b) input profile with amplitude 50 mm. In comparison between results shown in Figures 31 and 32, the relative displacement is smaller in Figure 32. As expected, due to smaller

displacement is Figure 32, the linear system which has a larger stiffness compared to the nonlinear model has the lowest spring deflection (x) and therefore the smallest relative displacement (z).

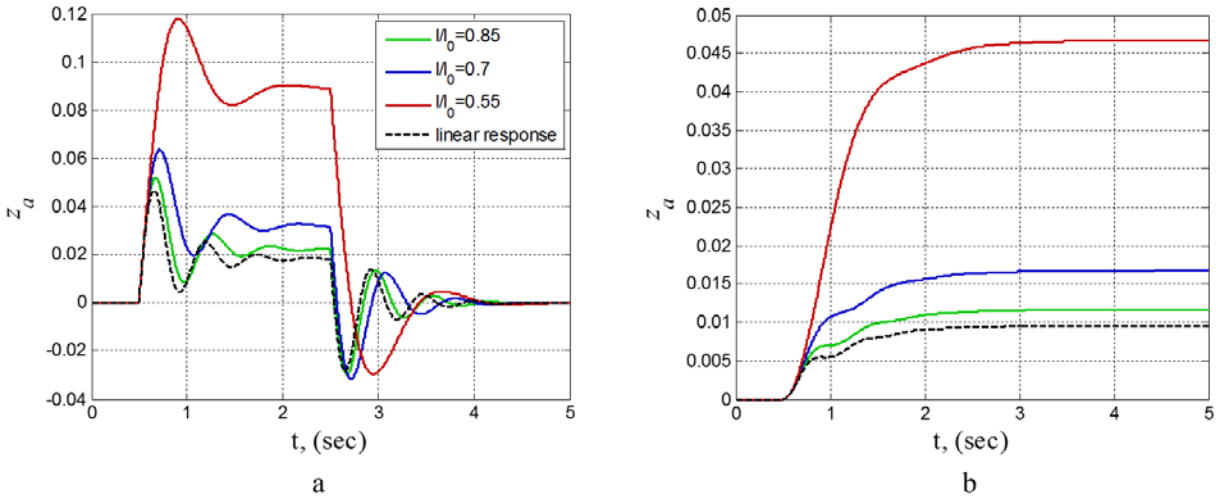

Figure 32: Motion control, step (a) and ramp (b) input profile with amplitude 50 mm

Therefore, it should be noted that improvement in motion control is dependent on the input amplitude. For example, Figure 33 shows that an increase in the input amplitude results in reduced motion control in nonlinear cases and therefore care should be taken in design to ensure that maximum motion control is achieved. For example if large input profile is expected the stiffness of both side springs and vertical spring should be increased accordingly. In Figure 33, $\bar{z}_{max}$ is the maximum peak to peak relative displacement normalized by the maximum base peak to peak motion.

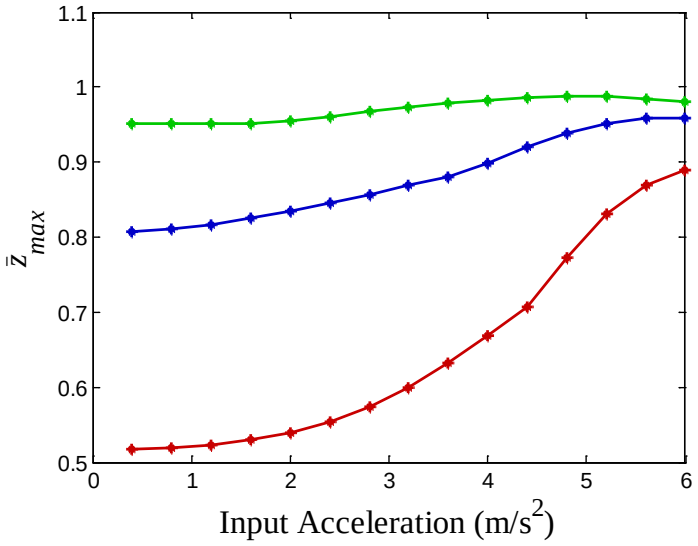

Figure 33: Maximum displacement; Green ($^{l}/_{l_0} = \mathbf{0.85}$), Blue ($^{l}/_{l_0} = \mathbf{0.7}$)), Red ($^{l}/_{l_0} = \mathbf{0.55}$)

In order to evaluate the system isolation, acceleration applied to the mass is plotted in Figures 34 and 35. The input amplitude in Figure 34 and 35 is 0.1 $^{m}/_{s^2}$, and 6 $^{m}/_{s^2}$ respectively.

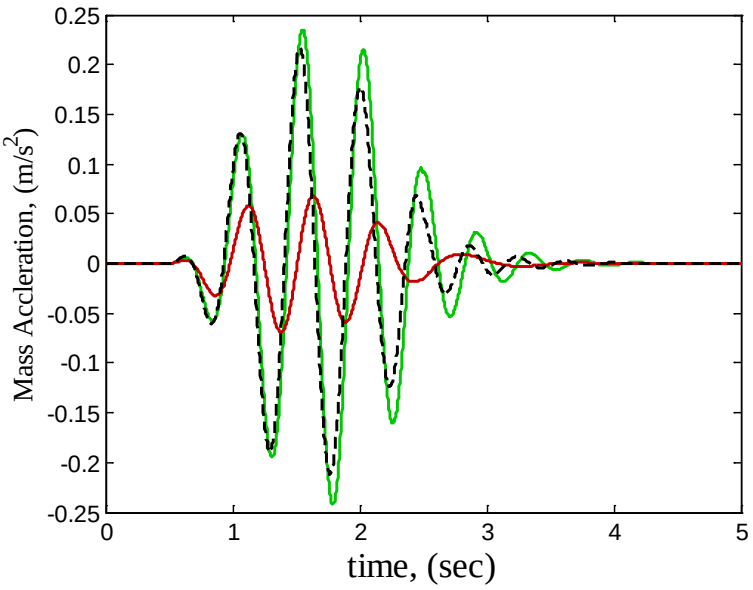

Figure 34: Mass acceleration; Black (linear), Green ($^{l}/_{l_0} = \mathbf{0.85}$), Red ($^{l}/_{l_0} = \mathbf{0.55}$)

Due to the lowered stiffness at the equilibrium point, isolation is improved when the operating range of the SDOF model is small however an increase in the input amplitude results in an increase in the operating range of the system. As shown in equation 18, with an increase in the operating range the overall stiffness of the system increases. This increase in the overall system stiffness results in reduced isolation for nonlinear systems as shown in Figure 35.

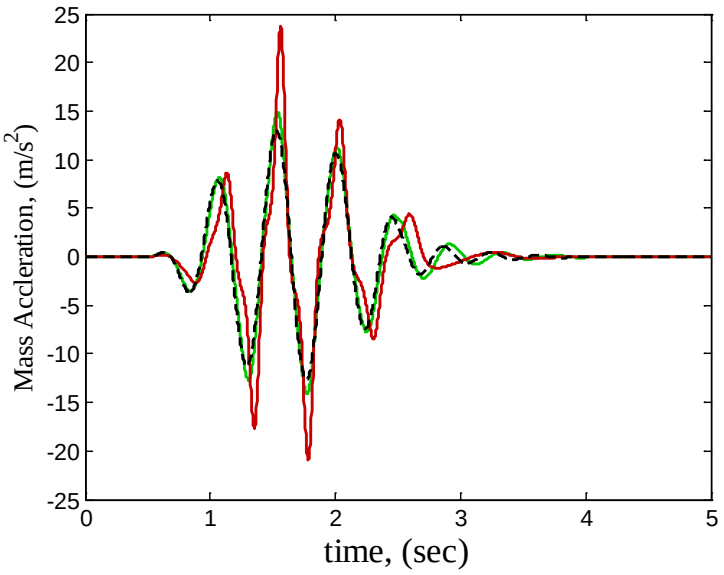

Figure 35: Mass acceleration; Black (linear), Green ($^{l}/_{l_0} = \mathbf{0.85}$), Red ($^{l}/_{l_0} = \mathbf{0.55}$)

A comparison of the response of the nonlinear systems in Figures 34 and 35 show that under small amplitude inputs, increased compression results in improved isolation as the equivalent stiffness is reduced. However, as the input amplitude is increased the operating range increases which results in greater equivalent stiffness and therefore isolation is reduced.

6.2. Side spring study:

Another parameter which can alter the performance of the mathematical model is the stiffness of the side spring. An increase in the stiffness of the side spring results in larger reduction in

stiffness at the equilibrium point. The increase in stiffness away from the equilibrium point is also faster for the case with greater stiffness. A comparison between Figures 30 and 36 shows that changing the stiffness of the side spring and the pre-compression results in similar qualitative change in the performance of the device. Increasing the amount of pre-compression or stiffness of the side springs results in a larger reduction in stiffness at the equilibrium point while it causes a faster increase in stiffness away from the equilibrium point.

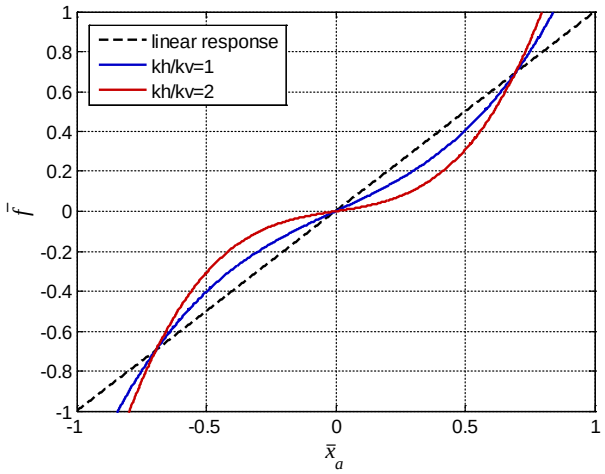

Figure 36: Force deflection, stiffness study

The system response to the acceleration input shown in Figure 28 with amplitude of 1 $^{m}/_{s^2}$, is studied. Figure 37 compares the displacement output of two different nonlinear models against the equivalent linear system with stiffness k_v, which shows improved motion control for nonlinear cases as the stiffness of the side spring increases.

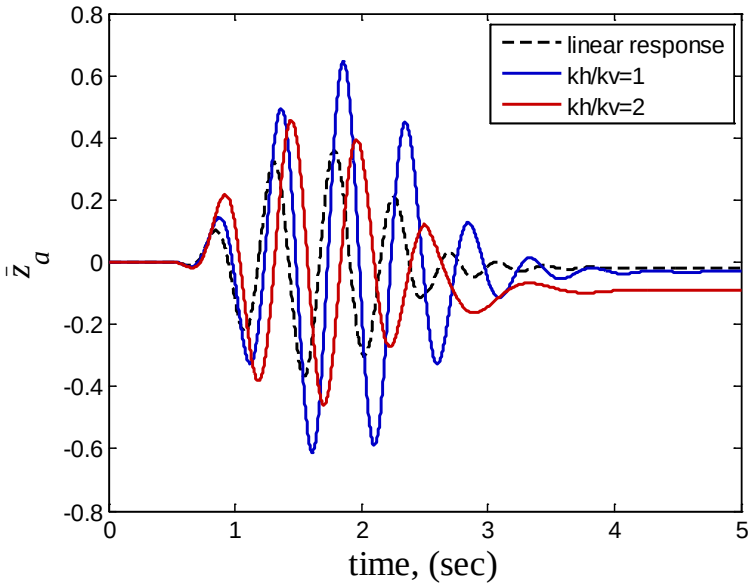

Figure 37: Motion control, stiffness study

However, it should be noted that improvement in motion control is dependent on the input amplitude. For example, Figure 38 shows that an increase in the input amplitude results in reduced motion control in nonlinear cases and therefore care should be taken in design to ensure that motion is reduced.

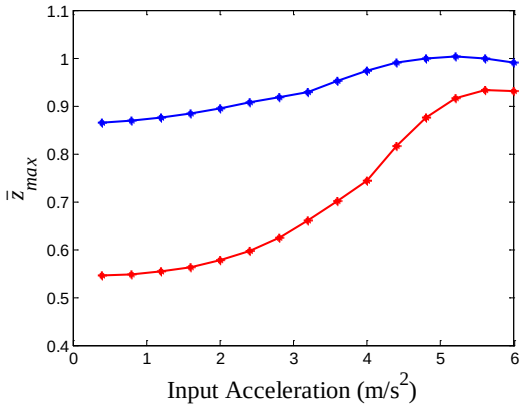

Figure 38: Maximum displacement; Blue ($^{k_h}/_{k_v} = 1$)), Red ($^{k_h}/_{k_v} = 2$)

In order to evaluate the system isolation, acceleration applied to the mass is plotted in Figures 39 and 40. The input amplitude in Figure 39 and 40 is 0.1 $^{m}/_{s^2}$, and 6 $^{m}/_{s^2}$ respectively.

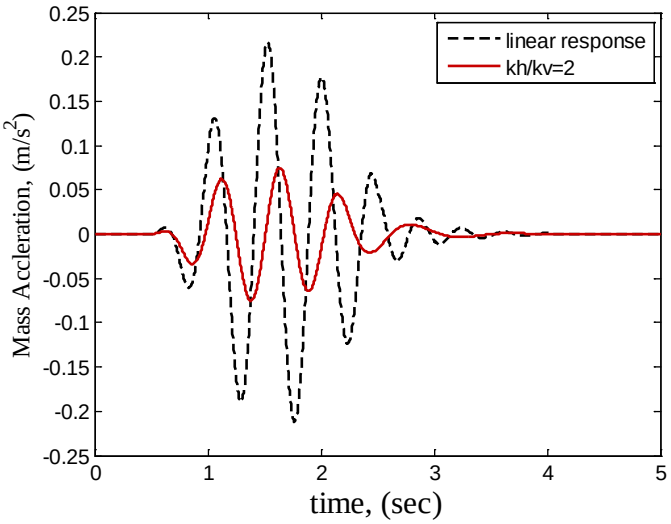

Figure 39: Mass acceleration, Input amplitude: 0.1 $^{m}/_{s^2}$

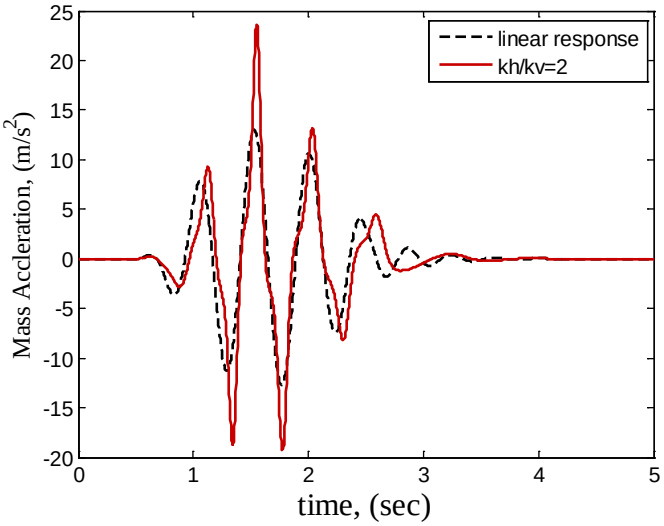

Figure 40: Mass acceleration, Input amplitude: 6 $^{m}/_{s^2}$

A comparison of the Figures 39 and 40 shows that an increase in the input amplitude results in reduced isolation for the nonlinear system as the operating range of the mechanism is increased, resulting in a larger equivalent stiffness.

6.3. Spring length study:

Another parameter which can alter the performance of the mathematical model is the free length of the side spring. In Figure 41, ratio of the spring length at equilibrium to the spring free length is , $\frac{l}{l_0} = 0.6$. The reduction in stiffness at the equilibrium point is the same for all three spring lengths however with the increase in spring length the increase in stiffness away from the operating point becomes more gradual. The most favorable combination is seen in the shortest side spring as stiffness of the model is lowered at the equilibrium point, allowing the spring to deflect, while stiffness is increased away from the equivalent point preventing large deformations.

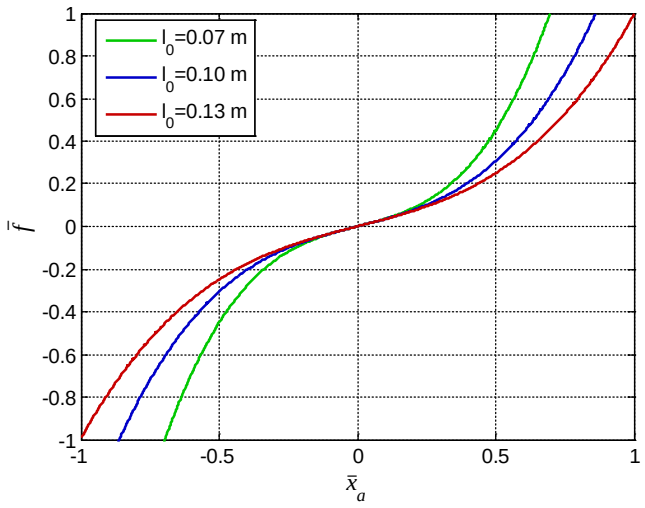

Figure 41: Force deflection, spring length study

The system response to the acceleration input shown in Figure 28 with amplitude of 4 $^{m}/_{s^2}$, is studied. Figure 42 compares the displacement output of three different nonlinear models against the equivalent linear system with stiffness k_v, which shows better motion control for linear model. Due to the introduction of the side springs, the equivalent stiffness of the model at the equilibrium is reduced. Reduction in stiffness results in larger displacement, however comparing the results for the two nonlinear cases in Figure 42 shows that due to the faster increase in stiffness away from the equilibrium point, the model with the shorter spring length provides better motion control.

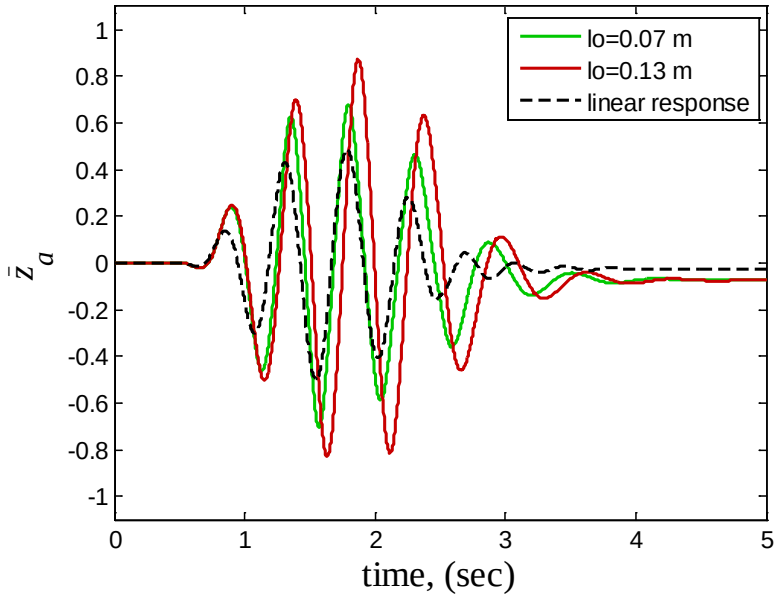

Figure 42: Motion control, spring length study

However, it should be noted that improvement in motion control is dependent on the input amplitude. For example, Figure 43 shows that an increase in the input amplitude results in reduced motion control in nonlinear cases and therefore care should be taken in design to ensure that maximum motion control is achieved.

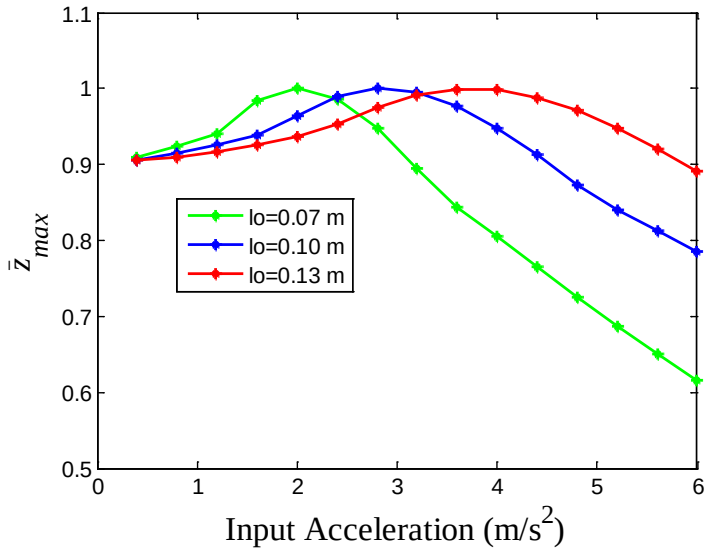

Figure 43: Maximum displacement

In order to evaluate the system isolation, acceleration applied to the mass is plotted in Figures 44 and 45. The input amplitude in Figures 44 and 45 is 2 $^{m}/_{s^2}$, and 4 $^{m}/_{s^2}$ respectively.

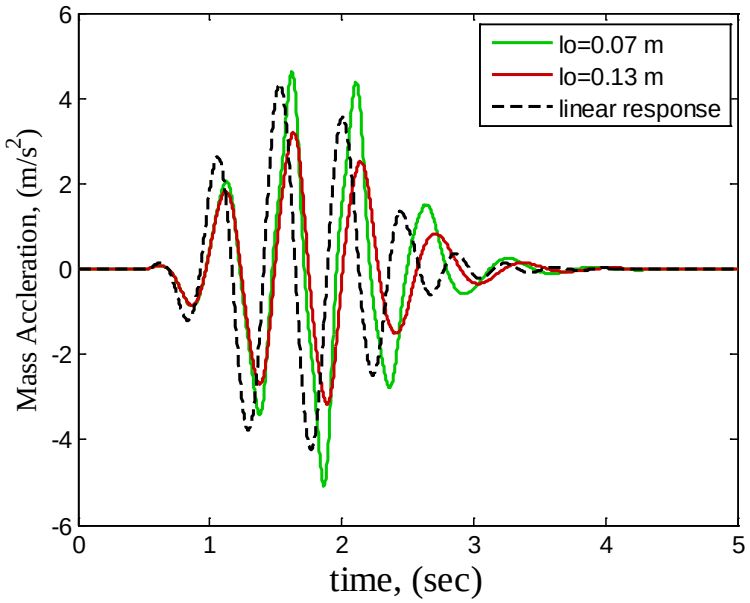

Figure 44: Mass acceleration, Input amplitude: 2 $^{m}/_{s^2}$

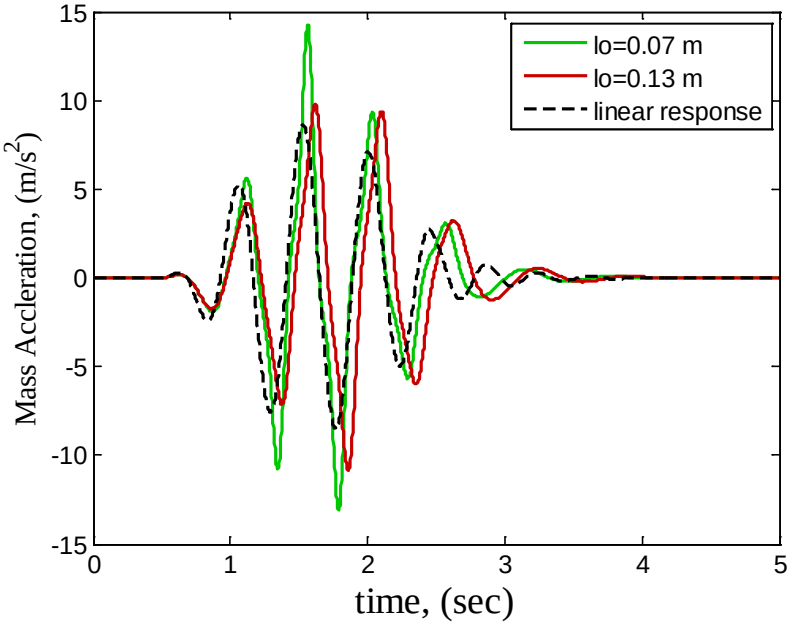

Figure 45: Mass acceleration, Input amplitude: 4 $^{m}/_{s^2}$

A comparison of the Figures 44 and 45 shows that an increase in the input amplitude results in reduced isolation for the nonlinear system and therefore care should be taken in design to ensure that maximum isolation is achieved.

7. BEAM STRUCTURE FEM RESULTS AND DISCUSSION

Based on the design requirements, the nonlinear behavior of the beam may be controlled by adjusting different parameters. For example, a change in the material to steel with elastic modulus, $E = 220 \times 10^9$Pa , and Poisson's ratio, $v = 0.32$ changes the behavior of the beam as shown in Figure 46. In the FEM for the steel beam the model is developed using the same steps outlined for the Aluminum beam. Due to the greater stiffness of steel compared to aluminum, the device can be made stiffer by using steel. Comparing the slope of the two lines in Figure 46 shows that the steel beam has a larger negative stiffness. This change in behavior is analogous to the change in behavior of the SDOF model shown in pre-compression study. Greater pre-compression

in the side springs, resulted in larger reduction in stiffness at equilibrium point while in the beam model, changing the material to steel resulted in greater negative stiffness and therefore larger reduction in stiffness at the equilibrium point.

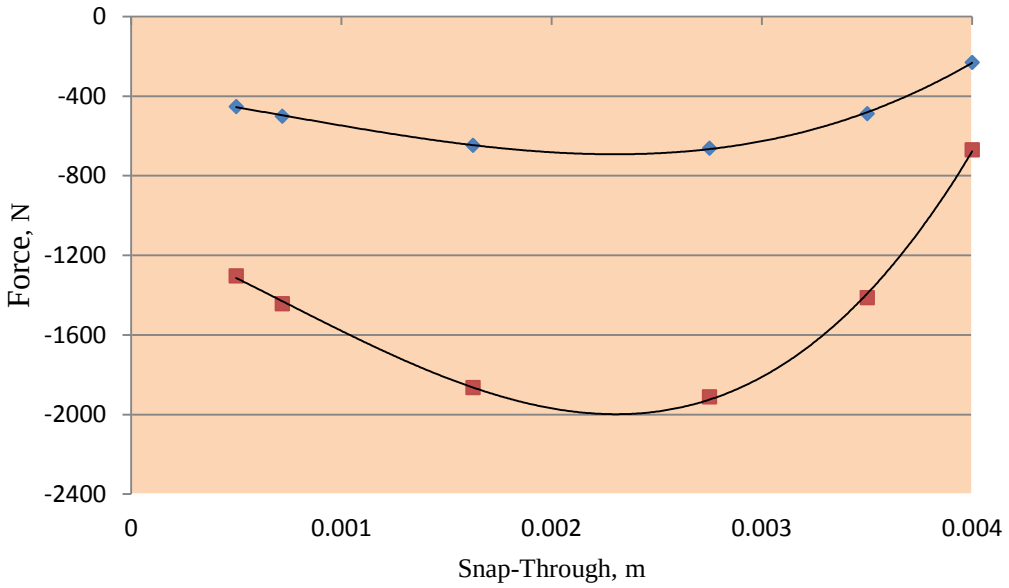

Figure 46: Nonlinear behavior of a snap-through beam; key: Red is for steel and blue is for Aluminum

Changing the geometry of the beam can also result in a change in the nonlinear behavior of the model. For example, changing the thickness of an Aluminum beam from 1 mm to 1.1 mm results in behavior as shown in Figure 47. Comparing the slope of the two lines in Figure 47 shows that the two beams have equal negative stiffness at the equilibrium point however the beam with thickness 1.1 mm has a greater negative stiffness away from the operating point. This change in behavior is analogous to the change in behavior of the SDOF model shown in the spring length study. As shown in Figure 41, changing the spring length in the SDOF model does not affect the reduction in the overall stiffness at the equilibrium point while reducing the size of the spring results in greater negative stiffness away from the operating point.

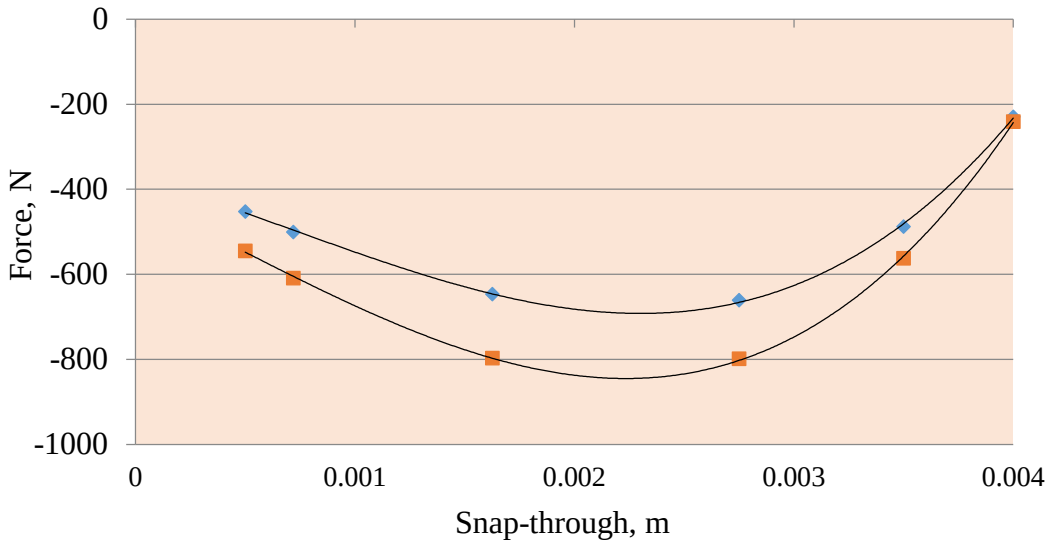

Figure 47: Nonlinear behavior of a snap-through beam; key: Orange is for thickness=1.1 mm and blue is for thickness=1.0 mm

Geometry of the beam can also be altered by changing the width of the beam. For example, reducing the width of an Aluminum beam from 5 mm to 4 mm results in behavior as shown in Figure 48. Comparing the slope of the two lines in Figure 48 shows that reducing the width of the beam results in reduction of the negative stiffness.

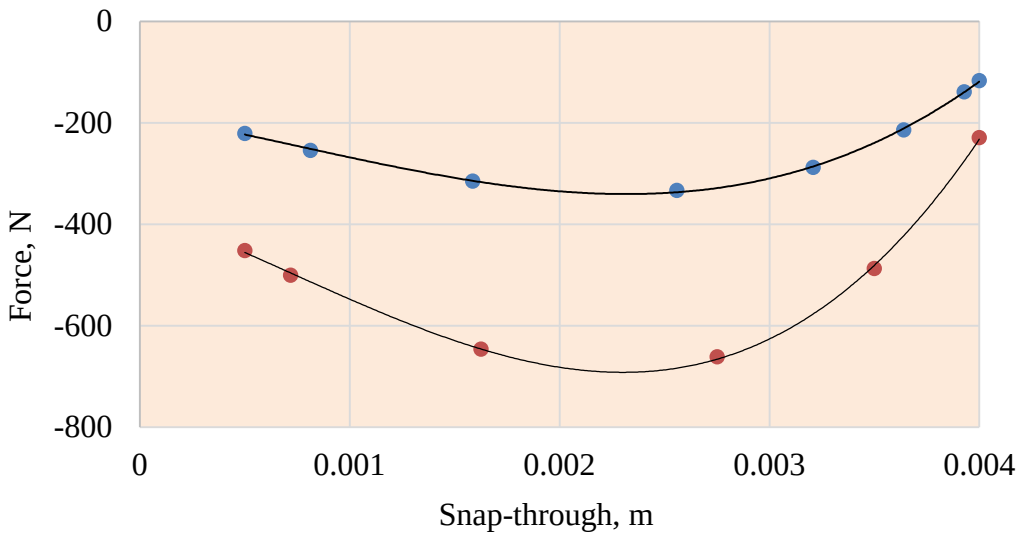

Figure 48: Nonlinear behavior of a snap-through beam; key: Red is for width=5 mm and blue is for width=4 mm

As was shown in Figure 18, due to the limited space available in seat suspensions for negative stiffness devices, using a single beam is not efficient. To improve the packaging and efficiency of the device, multiple beams are used to create a single device. As was shown in Figure 46, by changing the material for the beam, the nonlinear behavior of the model is altered. The change in the performance of a single beam can in turn alter the performance of the device. Figure 49 shows the behavior of a single device made from six beams generated following the steps outlined in section 4 (analysis of snap-through beam structure). Two data sets compare the performance of the device using Aluminum and Steel beams elements. Comparing the slope of the two lines shows that changing the material from Aluminum to Steel results in larger negative stiffness which in turn can further reduce the overall system stiffness at the equilibrium point.

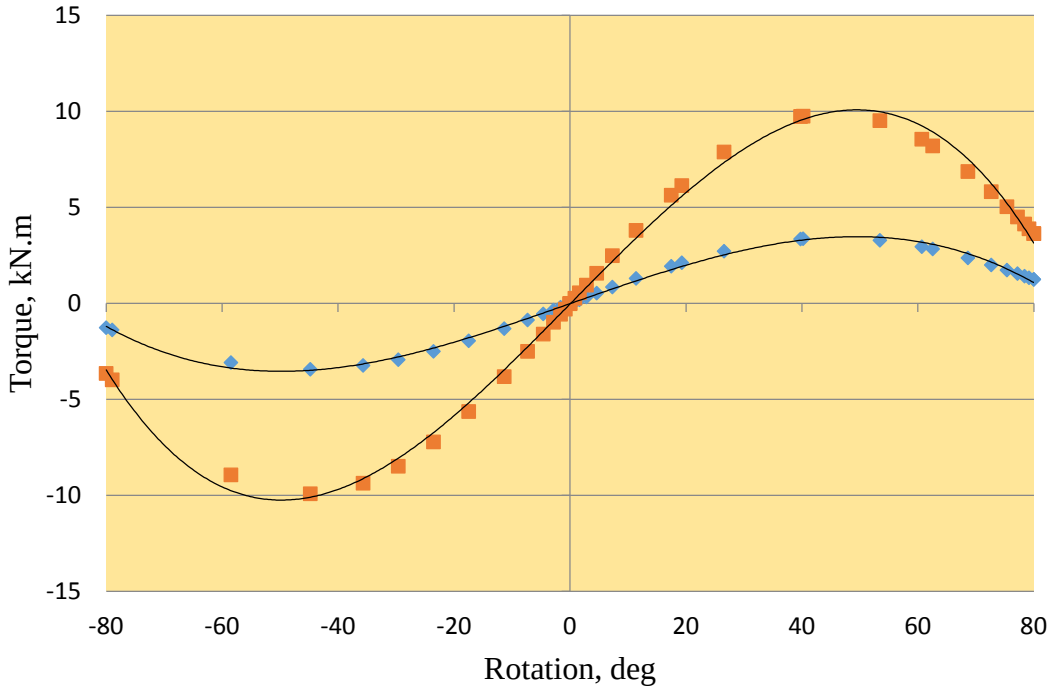

Figure 49: Nonlinear behavior of snap-through beam structure; key: Orange is for steel and blue is for Aluminum

As shown in Figures 47 and 48, changing the geometry of a beam can alter the performance a single beam. For example in Figure 47, it is shown that increasing the thickness of a single beam from 1 mm to 1.1 mm does not affect the reduction in the overall stiffness at the equilibrium point while the beam with larger thickness has a larger negative stiffness away from the operating point. Changing the thickness of the beam can have similar effects in devices with multiple beams. Figure 50 compares the performance of two devices each made from six Aluminum beams as shown in Figure 18. Comparing the slopes of two lines in Figure 50, it can be shown that increasing the thickness of the beams does not affect the stiffness at the equilibrium point. However, using beams with larger stiffness results in greater reduction in overall stiffness away from the operating point.

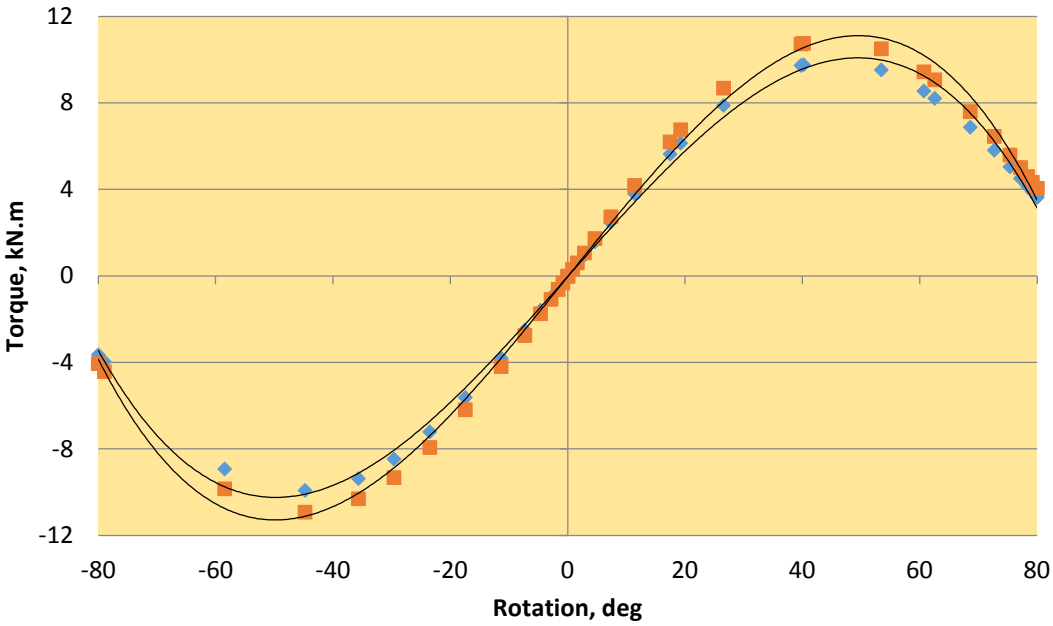

Figure 50: Nonlinear behavior of a snap-through beam structure; key: Orange is for thickness=1.1 mm and blue is for thickness=1.0 mm

8. CONCLUSION

A literature and patent review is conducted for seat suspension designs that exploit a negative stiffness device for isolation improvement. Next, a finite element model (FEM) for a nonlinear snap-through beam is developed, analyzed and compared to a model of nonlinear spring components with snap-through developed from a combination of thin beam elements. The thin beam structure is analyzed using finite element software (ABAQUS/CAE [4]). Based on prior work by Gunston et al. [2], different design parameters, such as the beam geometry, are altered to study effects on overall system performance.

First by increasing the stiffness of the material it is seen that the reduction in stiffness around the operating point is larger and the subsequent increase in the overall stiffness is sharper. Next, the geometry of beam elements is altered by changing the thickness and width of the elements.

Using components of a seat suspension, a SDOF system model with geometric nonlinearity is developed. Parametric study is conducted to analyze the effect that certain geometric and

mechanical properties of the nonlinear springs may have on system responses in time domain. Specifically, the pre-compression, lengths, and ratio of horizontal to vertical spring rates are considered. It is shown that a change in the nonlinear SDOF system model (by altering the stiffness and pre-compression in the side springs) is analogous to changing the stiffness of beam elements in the snap-through device. Also a change in the SDOF system model (by changing the size of the side springs) is analogous to changing the thickness of beam elements in the snap-through device.

Using the simple SDOF system model, the dynamic response of the system is studied. In order to achieve better motion control and isolation in time domain, systems with greater reduction in stiffness at the equilibrium point and sharper increase in stiffness away from the equilibrium point should be considered. However, a large reduction in the stiffness around the operating point could result in higher static deflection. The combination of reduced stiffness at operating point and sharp increase in stiffness away from operating point may also induce unfavorable results when input amplitude is increased. Under large amplitude inputs, an increase in stiffness away from the operating point can shift the fundamental frequency of the system toward higher frequencies and thus reduce the range of frequencies under which vibration isolation is achieved.

9. RECOMMENDATION FOR FUTURE WORK

The top priority for future work will be to conduct experimental validation of the results obtained. The current model has provided some insight about the dynamic response of the experimental model. Also, the mathematical model used is a simple single degree of freedom and in the next steps additional degrees of freedom need to be considered in order to more accurately predict dynamic performance.

10. ACKNOWLEDGMENTS

I would first of all like to thank my advisor Dr. Scott Noll. He was always willing to take time out of his busy schedule and sit down with me and discuss the project, brainstorm ideas and give me valuable advice. My accomplishments over the last two years of my undergraduate studies are a result of his constant support, guidance and encouragement. There are not enough words for me to express my gratitude for his support.

I would also like to thank my advisor Prof. Rajendra Singh who provided me valuable feedback on my progress and allowed me to learn so much by joining the Acoustics and Dynamics laboratory. I would also like to thank all members of ADL for their support and encouragement.

Last but not least I would like to thank the College of Engineering for providing me with a scholarship for completing this research. I would also like to thank the instructor of Mechanical Engineering 4999H, Dr. Robert Siston, who provided me with much needed advice about completing my undergraduate research and building my professional skills.

11. SELECTED REFERENCES

[1] C. Lee, V. Goverdovskiy and A. Temnikov, "Design of seats with negative stiffness to improve vehicle driver vibration isolation," *Journal of sound and vibration*, no. 302, pp. 865-874, 2007.

[2] T. Gunston, J. Rebelle and M. Griffin, "A comparison of two methods of simulating seat suspension dynamic performance," *Journal of Sound and Vibration*, no. 278, pp. 117-134, 2004.

[3] D. L. Platus, "Negative stiffness mechanism vibration isolation systems," *Proceedings of the SPIE Vibration control in Microelectronics, Optics, and Metrology*, vol. 1619, pp. 44-54, 1991.

[4] Abaqus (version 6.13), Analysis User's Guide, Dassault Systems, Providence, RI, 2013

[5] V. Goverdovskiy, A. Temnikov, G. Furin and C. Lee, "Stiffness control mechanism for a compact seat suspension". Russia Patent 2,216,461, 2003.

[6] V. Goverdovskiy, B. Gyzatullin and V. Petrov, "Method of vibration isolation of a vehicle driver". Russia Patent 2,115,570, 1998.

[7] V. Goverdovskiy and C. Lee, "Method of stiffness control of a suspension for a vehicle driver compact seat". Russia Patent 2,214,335, 2003.

[8] A. Carrella, M. Brennan, T. Waters and V. J. Lopes , "Force and displacement transmissibility of a nonlinear isolator with high-static-low-dynamic-stiffness," *International Journal of Mechanical Sciences*, no. 55, pp. 22-29, 2012.